Effects of Baseline Conditions on the Simulated Hydrologic Response to Projected Climate Change

Kathryn M. Koczot*

CAWSC, U.S. Geological Survey, San Diego, California

Steven L. Markstrom and Lauren E. Hay

U.S. Geological Survey, Denver, Colorado

Received 20 August 2010; accepted 23 January 2011

ABSTRACT: Changes in temperature and precipitation projected from five general circulation models, using one late-twentieth-century and three twenty-first-century emission scenarios, were downscaled to three different baseline conditions. Baseline conditions are periods of measured temperature and precipitation data selected to represent twentieth-century climate. The hydrologic effects of the climate projections are evaluated using the Precipitation-Runoff Modeling System (PRMS), which is a watershed hydrology simulation model. The Almanor Catchment in the North Fork of the Feather River basin, California, is used as a case study.

Differences and similarities between PRMS simulations of hydrologic components (i.e., snowpack formation and melt, evapotranspiration, and streamflow) are examined, and results indicate that the selection of a specific time period used for baseline conditions has a substantial effect on some, but not all, hydrologic variables. This effect seems to be amplified in hydrologic variables, which accumulate over time, such as soil-moisture content. Results also indicate that uncertainty related to the selection of baseline conditions should be evaluated using a range of different baseline conditions. This is

* Corresponding author address: Kathryn M. Koczot, CAWSC, U.S. Geological Survey, 4165 Spruance Road, Suite 200, San Diego, CA 92101.

E-mail address: kmkoczot@usgs.gov

DOI: 10.1175/2011EI378.1

particularly important for studies in basins with highly variable climate, such as the Almanor Catchment.

KEYWORDS: Climate change; Baseline conditions; Downscaling; Precipitation-Runoff Modeling System

1. Introduction

In a recent study conducted by the U.S. Geological Survey, the hydrologic effects of different emission scenarios for the twenty-first century were evaluated for 14 basins in different hydroclimatic regions across the United States (see Hay et al. 2011). The Precipitation-Runoff Modeling System (PRMS) (see Leavesley et al. 1983), a process-based, distributed-parameter watershed model, was used to evaluate these hydrologic effects. For each of the 14 basins, simulated precipitation and temperature from five general circulation models (GCMs), using one current (late twentieth century) and three future (years 2001–99) emission scenarios (see Alley et al. 2007), were downscaled using the change-factor method. This method is a downscaling technique that imposes the change from coarse-scale GCM projections to baseline (current) conditions as measured at climate stations (see Hay et al. 2011; Arnell 2003a; Arnell 2003b; Arnell and Reynard 1996; Hay et al. 2000; Diaz-Nieto and Wilby 2005; Eckhardt and Ulbrich 2003; Pilling and Jones 1999; Prudhomme et al. 2002; Hay and McCabe 2010). Hay et al. (Hay et al. 2011) chose the time period from 1 October 1987 through 30 September 1999 [water years (WYs) 1988–99] as the baseline condition of their study because input data used in the 14 PRMS models overlapped this period. This baseline condition period is herein referred to by its center year, 1994.

Simulations of future hydrologic conditions, developed using downscaled GCM output and a hydrologic model, are subject to numerous sources of uncertainty (see Hay et al. 2011). These sources include the GCM models, the downscaling technique, and the hydrologic model. The representation of the physical processes of the atmosphere, model structure, and feedbacks within the climate system all introduce large uncertainties in the GCM outputs (see Alley et al. 2007). GCMs produce outputs at a very coarse spatial resolution compared to the spatial resolution used by the PRMS model. When the GCM output is downscaled to finer resolution, an additional source of uncertainty is introduced to the simulation. This uncertainty, however, may be small relative to the inherent uncertainty in the GCMs (see Fowler et al. 2007; Khan et al. 2006). In many cases, uncertainty in the GCM model has been shown to be consistently greater than uncertainty from the hydrologic model itself (see Prudhomme and Davies 2009).

In this study, we examine the range of uncertainty associated with the choice of baseline conditions in the change-factor downscaling procedure. The Almanor Catchment of the North Fork of the Feather River, California (Figure 1), was selected from the 14 basins used by Hay et al. (Hay et al. 2011). The hydrology of the Almanor Catchment is influenced by the phases of Pacific decadal oscillation (PDO) (see Koczot et al. 2005), which is a multidecadal temperature pattern that has been identified in the surface-water temperature of the Pacific Ocean (see Mantua et al. 1997). These multidecadal changes in Pacific Ocean surface-water temperatures influence multidecadal increases and decreases of temperature and precipitation over the Almanor Catchment (see Koczot et al. 2005; Dettinger et al.

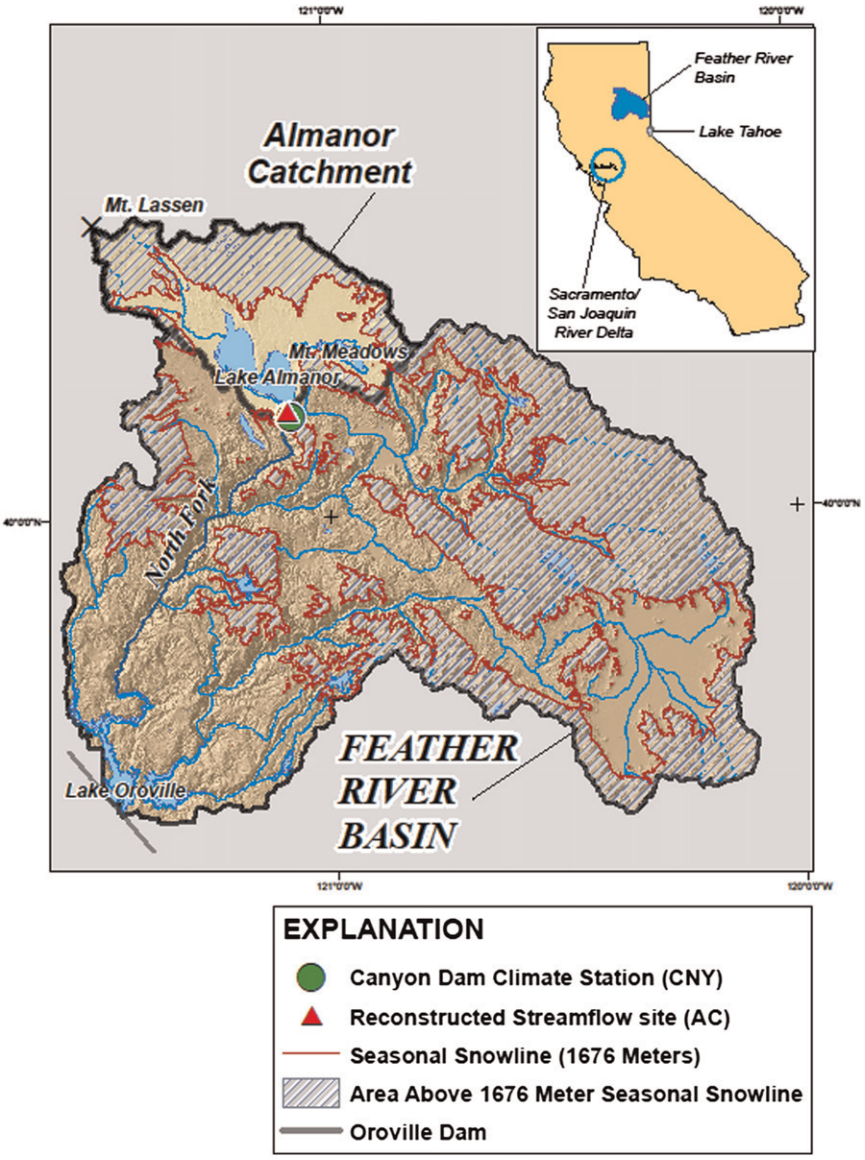

Figure 1. Location of the Almanor Catchment within the Feather River basin, California.

2004). In addition to the WYs 1988–99 baseline condition used by Hay et al. (Hay et al. 2011), baseline conditions representing a warm (WYs 1984–94) and a cool (WYs 1965–75) PDO phase were examined. Uncertainty caused by the selection of baseline conditions was evaluated using a comparison of PRMS simulation results obtained using the downscaled twenty-first-century climate projections.

2. Study area and historical hydroclimatology

The Almanor Catchment covers about 1295 km^2 of the 9324 km^2 Feather River basin (Figure 1). The Almanor Catchment comprises a series of small tributaries

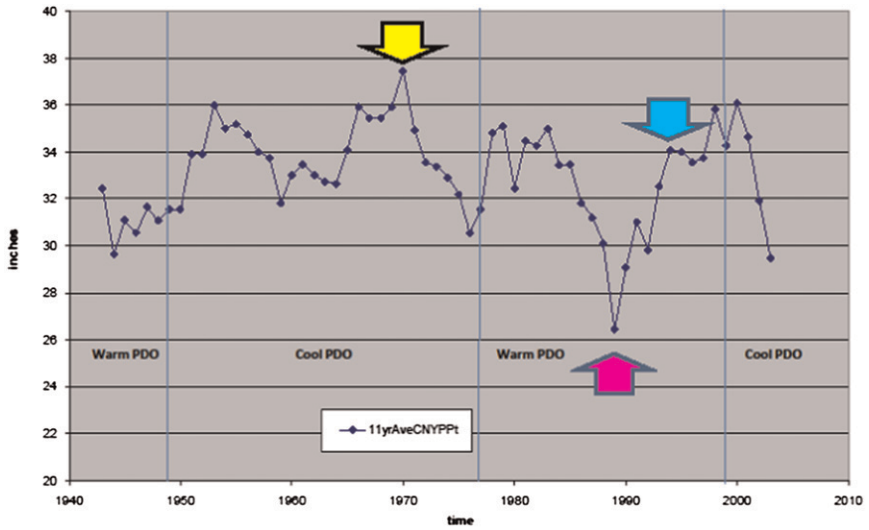

Figure 2. Precipitation measured at Canyon Dam plotted as 11-yr moving averages with the cool and warm PDO phases. Arrows indicate baseline condition 11-yr averages centered on the years 1994 (cyan), 1989 (magenta), and 1970 (yellow).

that drain meadows and surrounding mountains into two large lakes (Mountain Meadows and Almanor; Figure 1). The catchment is relatively unpopulated; however, it has been heavily developed for hydroelectric power generation. Vegetation cover is predominantly coniferous trees, with some areas of shrubs and grasses surrounding Mountain Meadows Lake. Elevations range from about 1310 m at the outflow below Lake Almanor to about 2896 m near Mt. Lassen; 50% of this catchment is below the historical seasonal snow line (Figure 1). Because of lower elevations and near-freezing winter conditions, precipitation form, snow accumulation, and snowmelt are sensitive to slight temperature variations. The catchment is underlaid by permeable and porous volcanic rocks (see Koczot et al. 2005). The high permeability of the volcanic rocks allows deep percolation of water and yields groundwater contributions to streams (see Durrell 1987).

The Almanor Catchment climate is Mediterranean, with cool wet winters and warm dry summers. Figure 2 shows the precipitation measured at Canyon Dam Climate Station, which is plotted as an 11-yr moving average, and the corresponding cool and warm phases of the PDO. Figure 3 shows the mean monthly streamflow (as simulated by PRMS) for the Almanor Catchment corresponding to two 11-yr periods identified in Figure 2 and centered on the years 1989 (magenta) and 1970 (yellow). The shift in the month of peak streamflow corresponds to the variability of the PDO (see Mantua et al. 1997), with cool PDO phases resulting in later peak streamflow and warm PDO phases resulting in an earlier peak streamflow (see Dettinger et al. 2004; Koczot et al. 2005). Peak timing of streamflow in the Almanor Catchment corresponds to variability of the PDO phases (Figure 3), with mean monthly peak streamflow occurring in May during the cool PDO phase (1970) and in February during the warm PDO phase (1989) (Figure 3).

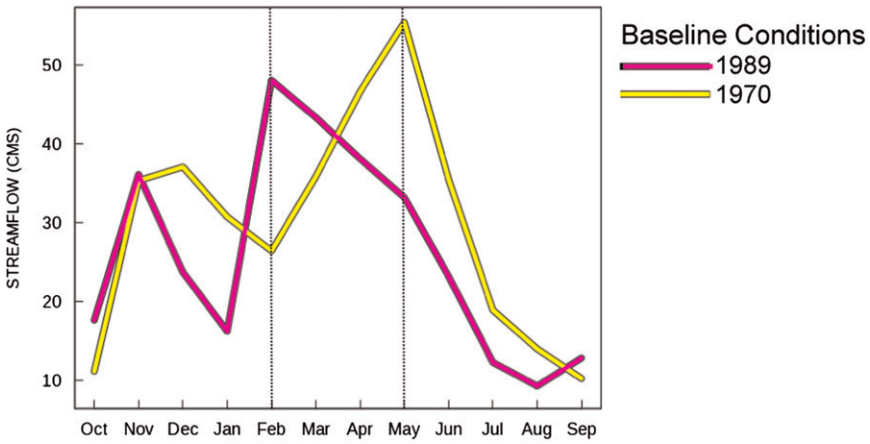

Figure 3. Mean monthly streamflow for baseline conditions 1989 (1984–94; magenta) and 1970 (1965–75; yellow).

3. Methods

The hydrologic model PRMS was used to evaluate the influence of baseline conditions on the hydrologic effects of projected climate change in the Almanor Catchment. The following three subsections describe 1) the PRMS model; 2) how the changes in climate, as projected by GCMs, were processed; and 3) the selection of three historical time periods, with each representing a different baseline condition.

3.1. Precipitation-Runoff Modeling System

This study uses PRMS (see Leavesley et al. 1983), a process-based, distributed-parameter watershed model. Input datasets are developed by partitioning a watershed into homogeneous hydrologic response units (HRUs), using characteristics such as slope, aspect, elevation, vegetation type, soil type, and precipitation distribution. PRMS requires daily inputs of precipitation and maximum and minimum air temperature. A water balance and an energy balance are computed daily for each HRU. PRMS simulates streamflow and related hydrologic components on a daily time step for each HRU and sums results for the whole basin (or, in this case, catchment). The PRMS application for the Almanor Catchment from Koczot et al. (Koczot et al. 2005) was used as the foundation model for this study. This application was modified from PRMS version 1998 and recalibrated to run using PRMS version 2010. Refer to Hay et al. (Hay et al. 2011) and Markstrom et al. (Markstrom et al. 2008) for further details on PRMS.

3.2. Changes in climate

Hay et al. (Hay et al. 2011) describe the generation of the climate-change input files. The PRMS model uses these files to simulate the hydrologic effects of the projected climate changes on the Almanor Catchment. GCM simulations of

Table 1. GCM outputs used in this study from the World Climate Research Programme's CMIP3 multimodel dataset archive. CMIP3 GCM documentation, references, and links can be found online (at http://www-pcmdi.llnl.gov/ipcc/model_documentation/ipcc_model_documentation.php). GCM definitions not expanded in the text: Bjerknes Centre for Climate Research Bergen Climate Model (BCC-BCM2.0), Commonwealth Scientific and Industrial Research Organisation Mark version 3.0 (CSIRO Mk3.0), Institute of Numerical Mathematics Coupled Model, version 3.0 (INM-CM3.0), and Model for Interdisciplinary Research on Climate 3.2 (MIROC3.2).

GCM	Description
BCC-BCM2.0	Bjerknes Centre for Climate Research, Norway
CSIRO Mk3.0	Australia Commonwealth Scientific and Industrial Research Organisation, Australia
CSIRO Mk3.5	Australia Commonwealth Scientific and Industrial Research Organisation, Australia
INM-CM3.0	Institute for Numerical Mathematics, Russia
MIROC3.2	National Institute for Environmental Studies, Japan

future climate were obtained from the World Climate Research Programme's Coupled Model Intercomparison Project phase 3 (CMIP3) multimodel dataset archive, which is referenced in the Intergovernmental Panel on Climate Change (IPCC) Fourth Assessment Report Special Report on Emission Scenarios (SRES; see Alley et al. 2007). Table 1 lists the five GCMs chosen for the study, and Table 2 describes the GCM baseline and three future (2001–99) emission scenarios chosen for analysis.

Projected precipitation and maximum and minimum temperature from the five GCMs (Table 1), using one current (late twentieth century) and three future (years 2001–99) emission scenarios (Table 2), were downscaled using the change-factor method (Figure 4). Mean monthly climate-change factors (percentage changes in precipitation and degree changes in temperature) were computed for 12-yr moving periods (from 2001 to 2099) using the 20C3M (current conditions) and the A2, B1, and A1B emission scenarios (Table 2). The climate-change input files for use with PRMS were generated by modifying the WYs 1988–99 baseline condition (selected from twentieth-century climate) (i.e., precipitation and maximum and minimum temperature) inputs with the mean monthly climate-change factors derived from the GCM model output. The first year of each 12-yr simulation was used as an initialization period for the PRMS model and was not included in the analysis of results; the median year from the last 11 years of each 12-yr period was used to

Table 2. GCM baseline and future emission scenarios chosen for this study (from Alley et al. 2007).

Emission scenario	Description/assumptions
20C3M	Twentieth-century climate used to determine baseline (1988–99) conditions
B1	Convergent world, with the same global population as emission scenario A1B but with more rapid changes in economic structures toward a service and information economy that is more ecologically friendly
A1B	Very rapid economic growth, a global population that peaks in the mid-twenty-first century, and rapid introduction of new and more efficient technologies with a balanced emphasis on all energy sources
A2	Very heterogeneous world with high population growth, slow economic development, and slow technological change

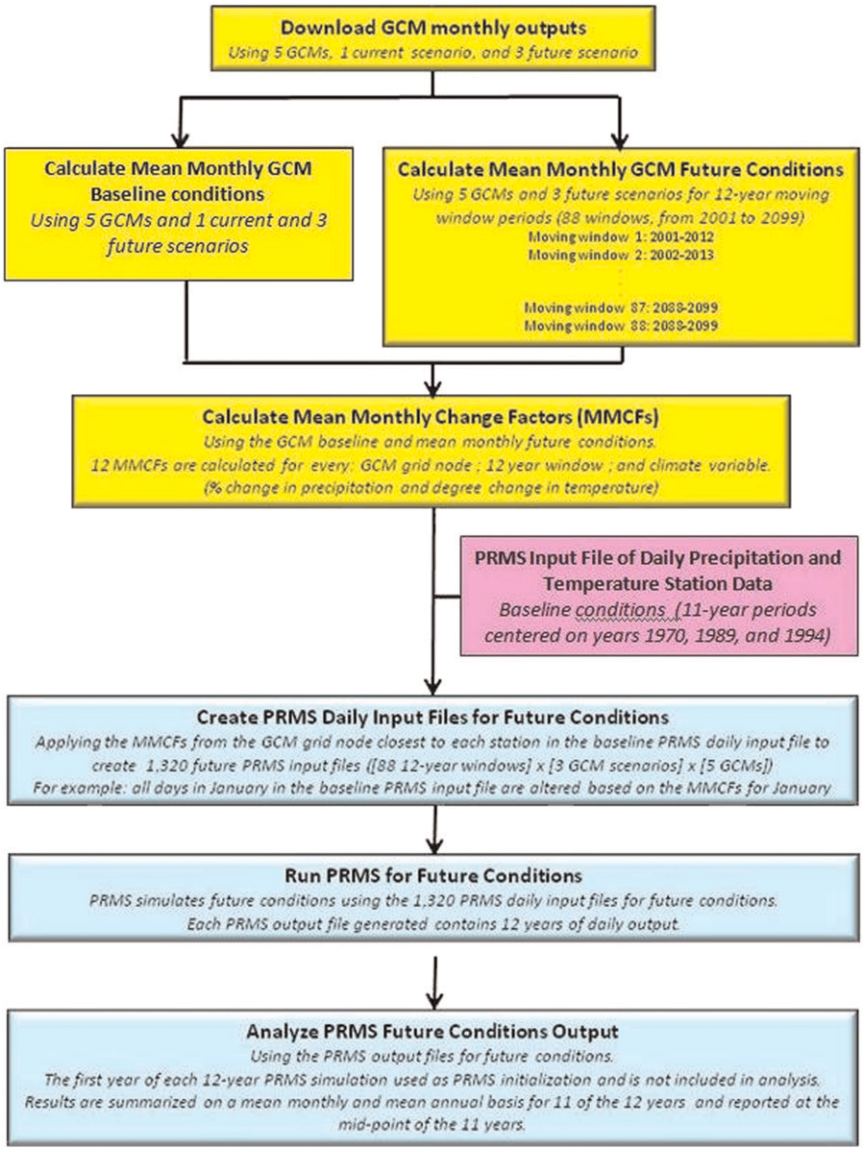

Figure 4. Schematic of the climate-change-factor method as applied in this study (from Hay et al. 2011).

reference (or label) the period. Figure 4 shows a schematic of the climate-change-factor method as applied in this study.

3.3. Baseline conditions

The hydrology in the Almanor Catchment is influenced by PDO phases (see Figures 2, 3). In addition to the baseline climatic condition chosen by Hay et al. (Hay et al. 2011), baseline conditions representing a warm and a cool PDO phase were examined.

Hay et al. (Hay et al. 2011) used WYs 1988–99 for a common baseline condition for the 14 basins in their study. This period, centered on the year 1994, ended in 1999 because many of the GCM projections of current climatic conditions end in 1999. Water year 1988 was selected as the start of the baseline condition based on the periods of record for the Natural Resources Conservation Service's snow telemetry records used by PRMS. In the Almanor Catchment, this baseline period has higher than average precipitation and is in the final years of a warm PDO phase (cyan arrow in Figure 2). To capture a range in historical climate events and simulate broader ranges of uncertainty, two other baseline conditions were chosen to represent a cool PDO and a warm PDO phase. The baseline condition representing a cool PDO phase was selected by choosing an 11-yr period centered on the year 1970 (1964–75), the wettest year in a cool PDO phase (yellow arrow in Figure 2). The baseline condition representing a warm PDO was selected by choosing an 11-yr period centered on the year 1989 (1983–94), the driest year in a warm PDO phase (magenta arrow in Figure 2). The catchment's mean monthly temperature peaks in July and is at a minimum in December or January (Figures 5a,b). The catchment's mean monthly maximum precipitation occurs in November through March, with minimum precipitation occurring in July (Figure 5c). PRMS-simulated streamflow, using the 1994 centered baseline condition, produces mean monthly peak streamflow during the month of May, with a lesser peak in March (Figure 5d). PRMS-simulated streamflow, using the 1970 centered (cool PDO) baseline condition, produces a mean monthly peak streamflow during the month of May, which is a value greater than the peak produced using the 1994 baseline conditions (Figure 5d). PRMS-simulated streamflow, using the 1989 centered (warm PDO) baseline condition, produces mean monthly peak streamflow during the month of February, with a minor peak in November. This corresponds to the peaks in mean monthly precipitation and is 3 months earlier than that produced using the 1994 and 1970 baseline conditions (Figure 5d).

4. Results and discussion

The scope of this study is limited to catchment-wide, mean monthly, and mean annual climate-change analyses of PRMS daily output simulated for the twenty-first century. Values are computed for 11-yr moving averages. The maximum and minimum temperature and precipitation (PRMS model input) are examined first. The PRMS model output was then analyzed from three different hydrological perspectives: 1) snowmelt and the percentage of precipitation that falls as snow; 2) evapotranspiration (potential and actual) and related components (soil-moisture recharge, sublimation, and soil zone evapotranspiration); and 3) streamflow and flow components (surface, subsurface, and groundwater).

4.1. PRMS inputs

Figures 6–8 show the catchment's mean annual maximum and minimum temperature and precipitation for each baseline condition. The three solid colored lines

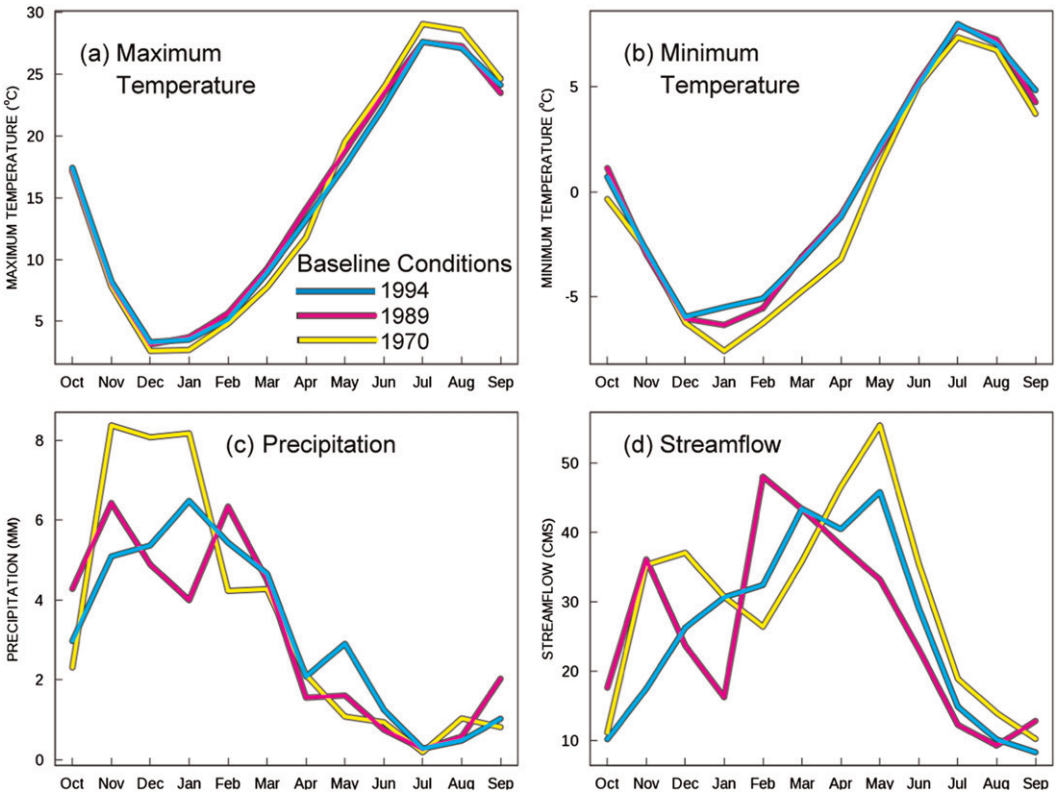

Figure 5. Almanor Catchment mean monthly (a) maximum temperature, (b) minimum temperature, (c) precipitation, and (d) streamflow for baseline conditions: 1994 (1989–99; blue), 1989 (1984–94; magenta), and 1970 (1965–75, yellow).

in Figures 6–8 indicate the 11-yr moving averages (x axis indicates the center year of the 11 years of the analysis period) for the three future emission scenarios (central tendencies of the five GCMs for A1B, A2, and B1). The blue, red, and yellow colors represent the A1B, A2, and B1 emission scenarios, respectively. The solid or hatched colored areas represent the range derived from the five GCMs, with the highest and lowest GCM projections forming the upper and lower bounds of the colored area. For details on how the ranges of uncertainty were calculated, see Hay et al. (Hay et al. 2011).

All applications of GCM projections show steady increases in temperature, with uncertainties associated with these projections increasing with time (indicated by the wide range of values among GCMs). The B1 scenario indicates the smallest changes for both maximum and minimum temperatures (Figures 6, 7). The amount of the initial jump from baseline conditions (black line) to the first moving average (2001–12) differs for each baseline period. Twenty-first-century temperature changes are projected to be the same magnitude for all baseline conditions because the change-factor downscaling method applies a similar change to each baseline.

Projected changes in mean annual precipitation are highly variable, showing increases and decreases in precipitation between GCM projections and within the

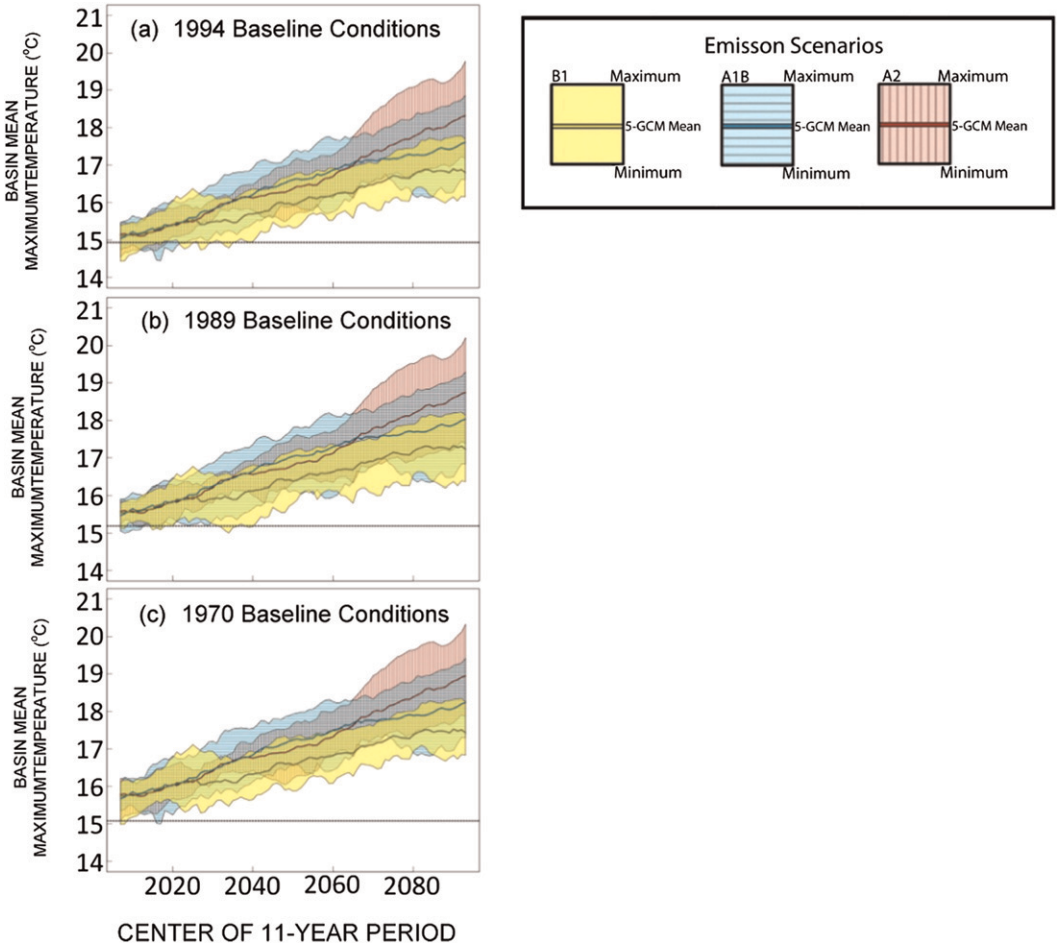

Figure 6. Projected range in 11-yr moving averages of maximum temperature by emission scenarios using the (a) 1994, (b) 1989, and (c) 1970 baseline conditions (black line).

emission scenario ranges (Figure 8). The projections of precipitation indicate both wetter and drier multidecadal cycles. These cycles are indicated in both the variation in the measured input data and the way the GCMs project climatic cycles for the three emission scenarios.

4.2. Snowmelt simulations

On a monthly basis, depending on the baseline conditions, simulated changes in snowmelt are quite variable (Figure 9). The box plots show by month the mean monthly values for the baseline (red lines) and the range in future conditions for five GCMs and three scenarios: 2030 (green), 2060 (tan) and 2090 (blue) (see Hay et al. 2011). The range of values indicated by the box plots illustrates the magnitude of simulated changes on a monthly basis for the five GCMs and three scenarios. Decreases in snowmelt are simulated from April through June, and

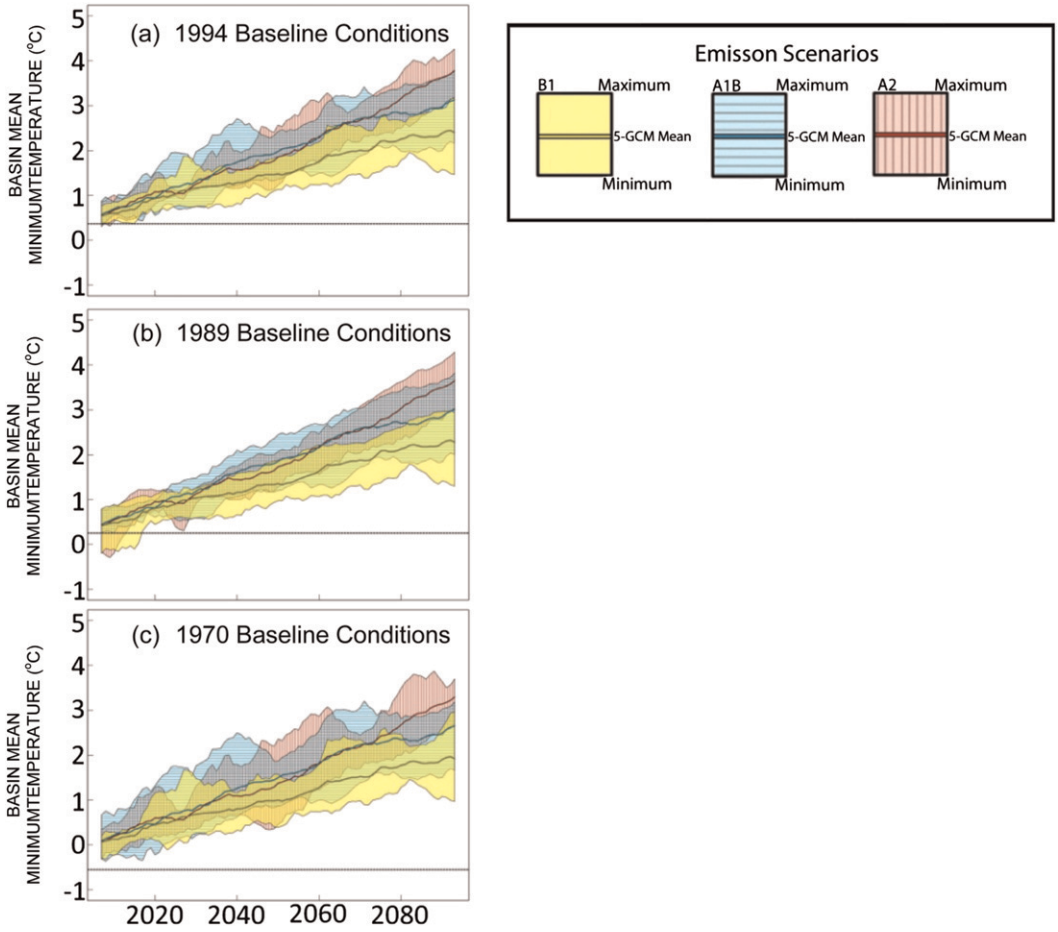

Figure 7. Projected range in 11-yr moving averages of minimum temperature by emission scenarios using the (a) 1994, (b) 1989, and (c) 1970 baseline conditions (black line).

increases are simulated for January for all baseline conditions by the end of the twenty-first century. By the end of the twenty-first century, peak timing of snowmelt is not simulated to change drastically when using the warm PDO baseline conditions (1994 and 1989; Figures 9a,b). In contrast, the cool PDO baseline conditions (1970) simulate a substantial change in peak snowmelt timing from May to January by the end of the twenty-first century (Figure 9c).

Twenty-first-century snowmelt simulations show a decrease in melt because winter temperatures are projected to increase, which will increasingly change the form of precipitation to rain. The amount of precipitation is not expected to change very much (Table 3), but wetter and drier multidecadal cycles seen in historical climate are expected to continue into the twenty-first century (Figure 8). Therefore, the simulated change in the proportion of total precipitation falling as snow for all baseline conditions show that by the end of the twenty-first century, precipitation in the Almanor Catchment will more likely fall in the form of rain rather than as snow (Figure 10), the warmer temperatures as projected by GCMs (Figures 6, 7)

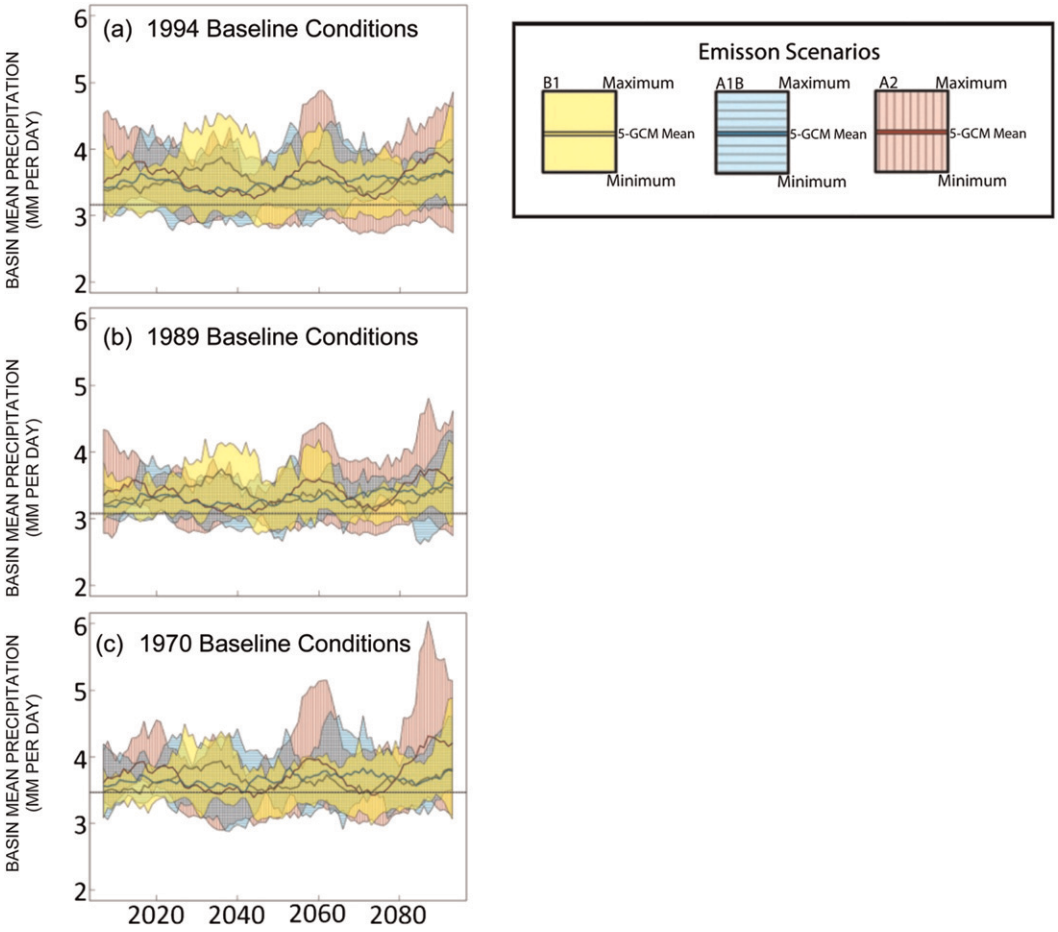

Figure 8. Projected range in 11-yr moving averages of precipitation by emission scenarios using the (a) 1994, (b) 1989, and (c) 1970 baseline conditions (black line).

will result in less snowfall, and less snowpack will remain to melt during the spring snowmelt season. Historically, peak streamflow in the Almanor Catchment has been dominated by snowmelt runoff. The simulations indicate that this will reduce the importance of the spring snowmelt to the stream and could eventually alter the characterization of the Almanor Catchment streamflow from being spring snowmelt dominated.

4.3. Evapotranspiration simulations

Simulations of evapotranspiration in the Almanor Catchment are affected by the seasonal timing of soil-moisture availability, vegetative life cycle (phenology), and potential evapotranspiration (PET). The wettest soil conditions occur in winter and spring during periods of maximum precipitation (Figure 5) and melting snowpack (Figure 9). Evapotranspiration peaks by April–May in response to soil-moisture

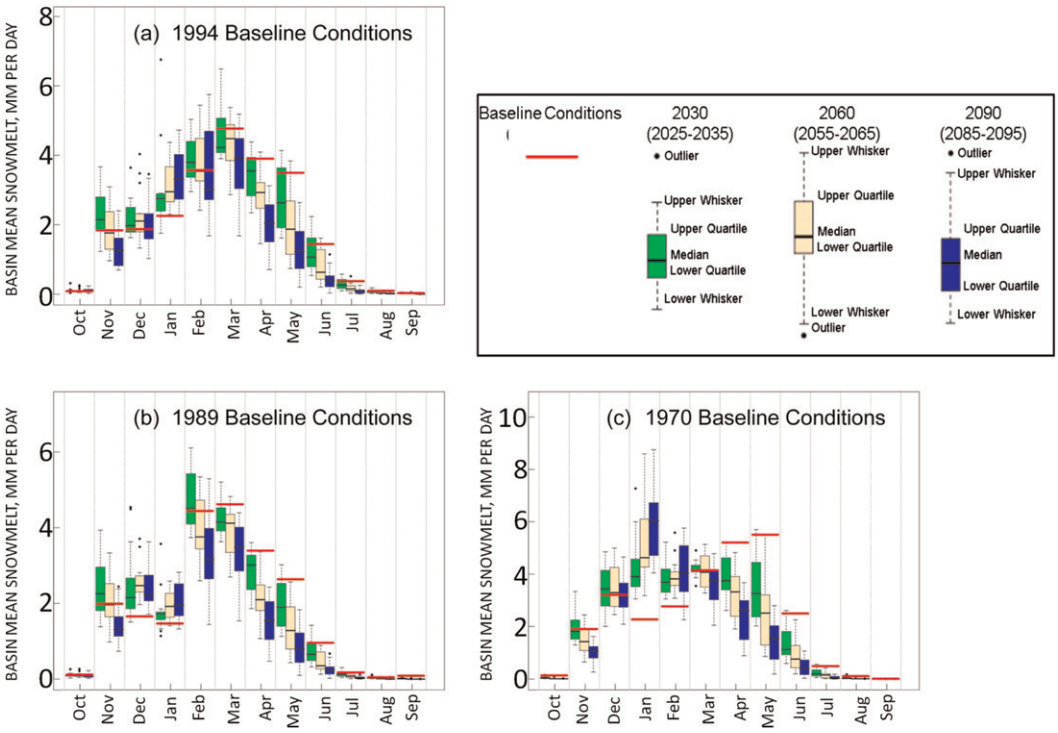

Figure 9. Mean monthly snowmelt and simulated ranges (2030, 2060, and 2090) using the five GCMs and three emission scenarios for the three baseline conditions: (a) 1994, (b) 1989, and (c) 1970.

availability, spring warming, and vegetative growth. Soil-moisture availability declines in early summer and limits evapotranspiration during the warmest months (Figure 5) (see Koczot et al. 2005). In PRMS simulations, once transpiration starts, transpiration is constrained by PET, soil-moisture availability, and the length of the growing season. PRMS simulations of evaporation (which includes sublimation; Figure 11c) are also constrained by PET (Figure 11a) and soil-moisture availability (not shown). Total actual evapotranspiration (AET; Figure 11e) is computed as the daily sum of sublimation, evaporation from retention on impervious surfaces, and soil zone evaporation and transpiration (see Markstrom et al. 2008).

The simulated change by emission scenario is shown for PET (Figure 11a); soil-moisture recharge (Figure 11b); sublimation (Figure 11c); soil zone evapotranspiration (Figure 11d); and AET (Figure 11a). Figure 11 shows the difference in the simulations based on the three baseline conditions. For purposes of this study, it is assumed land cover and vegetation types will remain the same throughout the twenty-first century. The simulated changes made from the B1 emission scenario projections in particular show that PET may level off by the end of the twenty-first century (Figure 11a). Simulated increases in AET are relatively small, especially for the 1970 (cool PDO) baseline condition (Figure 11e), even though simulated PET is expected to increase at much higher rates for all baseline conditions (Figure 11a).

Table 3. Twenty-first-century change in 11-yr moving averages (slope) and adjR2 based on the central tendencies of the five GCMs for the three emission scenarios by baseline condition. Italics indicates a significant negative trend, and bold indicates a significant positive trend ($p < 0.05$) accounting for lag-1 autocorrelation.

(a) Precipitation (mm)

	Emission scenario B1		Emission scenario A1B		Emission scenario A2	
Baseline condition	Slope	adjR2	Slope	adjR2	Slope	adjR2
1994	−0.0001	−0.01	0.0018	0.29	0.0013	0.02
1970	0.0001	−0.01	**0.0016**	**0.25**	0.0032	0.11
1989	−0.0008	0.01	**0.0025**	**0.45**	0.0019	0.07

(b) Max temperature (°C)

	Emission scenario B1		Emission scenario A1B		Emission scenario A2	
Baseline condition	Slope	adjR2	Slope	adjR2	Slope	adjR2
1994	**0.023**	**0.98**	**0.03**	**0.98**	**0.038**	**0.99**
1970	**0.023**	**0.98**	**0.03**	**0.98**	**0.038**	**0.98**
1989	**0.023**	**0.98**	**0.03**	**0.98**	**0.038**	**0.98**

(c) Min temperature (°C)

	Emission scenario B1		Emission scenario A1B		Emission scenario A2	
Baseline condition	Slope	adjR2	Slope	adjR2	Slope	adjR2
1994	**0.022**	**0.99**	**0.03**	**0.99**	**0.036**	**0.98**
1970	**0.022**	**0.99**	**0.03**	**0.99**	**0.036**	**0.98**
1989	**0.022**	**0.99**	**0.03**	**0.99**	**0.036**	**0.98**

(d) PET (mm)

	Emission scenario B1		Emission scenario A1B		Emission scenario A2	
Baseline condition	Slope	adjR2	Slope	adjR2	Slope	adjR2
1994	**0.0051**	**0.99**	**0.0072**	**0.98**	**0.0087**	**0.99**
1970	**0.0051**	**0.99**	**0.0071**	**0.98**	**0.0087**	**0.98**
1989	**0.0052**	**0.99**	**0.0073**	**0.98**	**0.0089**	**0.99**

(e) AET (mm)

	Emission scenario B1		Emission scenario A1B		Emission scenario A2	
Baseline condition	Slope	adjR2	Slope	adjR2	Slope	adjR2
1994	0.0012	0.63	**0.0012**	**0.89**	**0.0014**	**0.71**
1970	0.0002	0.05	0.0002	0.11	0.0001	−0.01
1989	0.0009	0.52	**0.001**	**0.84**	0.0011	0.64

(f) Streamflow ($m^3\ s^{-1}$)

	Emission scenario B1		Emission scenario A1B		Emission scenario A2	
Baseline condition	Slope	adjR2	Slope	adjR2	Slope	adjR2
1994	−0.0128	0.03	0.0111	0.08	0.0023	−0.01
1970	0.002	−0.01	0.0218	0.27	0.0452	0.15
1989	−0.0192	0.08	0.0229	0.3	0.0134	0.02

Table 3. (*Continued*)

(g) Surface flow ($m^3\ s^{-1}$)

	Emission scenario B1		Emission scenario A1B		Emission scenario A2	
Baseline condition	Slope	adjR2	Slope	adjR2	Slope	adjR2
1994	−0.000 36	0	0.000 76	0.14	0.000 94	0.03
1970	0.000 49	0.02	0.001 82	0.25	0.003 29	0.21
1989	−0.000 99	0.06	**0.001 09**	**0.33**	0.001 19	0.1

(h) Subsurface flow ($m^3\ s^{-1}$)

	Emission scenario B1		Emission scenario A1B		Emission scenario A2	
Baseline condition	Slope	adjR2	Slope	adjR2	Slope	adjR2
1994	0.005 61	0	**0.028 94**	**0.52**	0.0281	0.11
1970	0.019 66	0.15	**0.041 24**	**0.66**	0.070 67	0.39
1989	0.002 85	−0.01	**0.041 26**	**0.7**	0.040 05	0.26

(i) Groundwater flow ($m^3\ s^{-1}$)

	Emission scenario B1		Emission scenario A1B		Emission scenario A2	
Baseline condition	Slope	adjR2	Slope	adjR2	Slope	adjR2
1994	−0.018 05	0.79	−0.018 61	0.85	−0.026 78	0.79
1970	−0.018 12	0.75	−0.021 25	0.92	−0.028 71	0.81
1989	−0.021 09	0.83	−0.019 46	0.89	−0.027 84	0.85

(j) Precipitation that falls as snow (%)

	Emission scenario B1		Emission scenario A1B		Emission scenario A2	
Baseline condition	Slope	adjR2	Slope	adjR2	Slope	adjR2
1994	−0.18	0.97	−0.21	0.96	−0.27	0.99
1970	−0.2	0.96	−0.24	0.96	−0.31	0.99
1989	−0.18	0.98	−0.21	0.97	−0.26	0.99

(k) Snow-covered area (%)

	Emission scenario B1		Emission scenario A1B		Emission scenario A2	
Baseline condition	Slope	adjR2	Slope	adjR2	Slope	adjR2
1994	−0.16	0.96	−0.18	0.97	−0.23	0.98
1970	−0.17	0.97	−0.2	0.98	−0.25	0.98
1989	−0.16	0.97	−0.17	0.97	−0.22	0.98

(l) Snowpack water equivalent (mm)

	Emission scenario B1		Emission scenario A1B		Emission scenario A2	
Baseline condition	Slope	adjR2	Slope	adjR2	Slope	adjR2
1994	−0.65	0.91	−0.66	0.91	−0.86	0.9
1970	−0.87	0.93	−0.92	0.94	−1.16	0.92
1989	−0.62	0.93	−0.59	0.93	−0.74	0.93

Table 3. (*Continued*)

(m) Snowmelt (mm)						
	Emission scenario B1		Emission scenario A1B		Emission scenario A2	
Baseline condition	Slope	adjR2	Slope	adjR2	Slope	adjR2
1994	−0.0078	0.81	−0.0085	0.9	−0.0119	0.88
1970	−0.0064	0.76	−0.0069	0.88	−0.0097	0.78
1989	−0.0076	0.83	−0.0079	0.93	−0.0103	0.9

PRMS simulations of evapotranspiration variables, corresponding to the 1970 baseline condition (cool PDO), indicate some similarities and some substantial differences with evapotranspiration variables simulated using the 1989 and 1994 baseline conditions (warm PDO). Simulations based on all baseline conditions show relatively similar changes in soil-moisture recharge (Figure 11b). Sublimation from snowpack (Figure 11c) is simulated to decrease in the twenty-first century; PRMS simulations using the cool PDO baseline condition (1970) indicate larger decreases by the end of the twenty-first century than those produced using the warm PDO baselines (1994 and 1989). AET (Figure 11e) and soil zone evapotranspiration (Figure 11d) are simulated to increase by the end of the twenty-first century with some variability; PRMS simulations using the cool PDO baseline

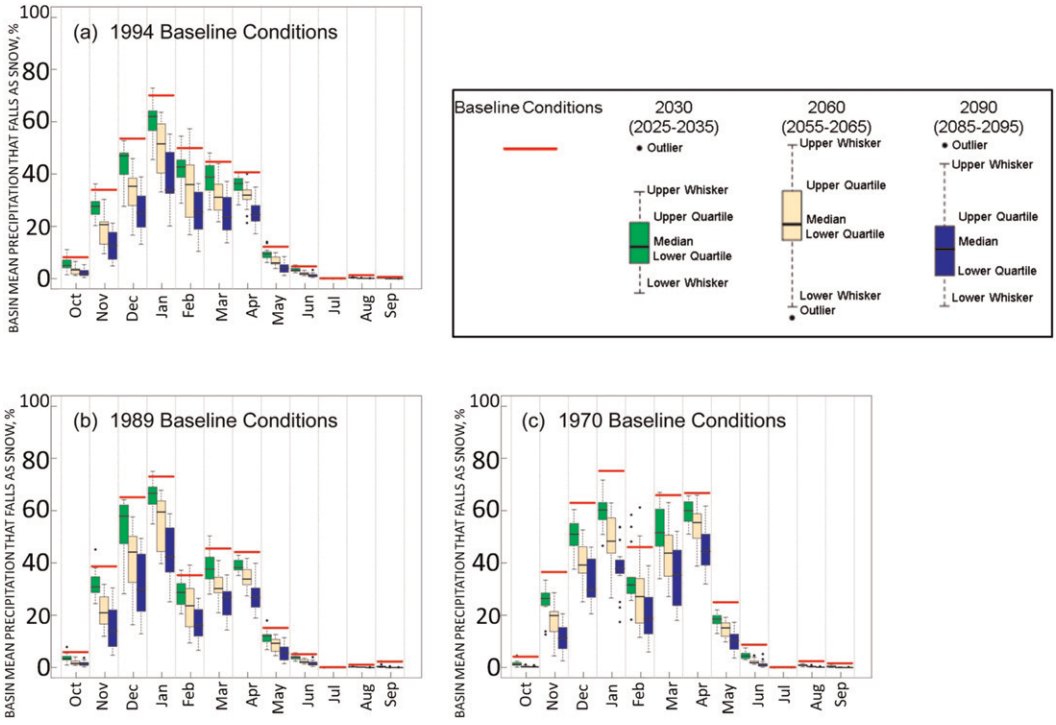

Figure 10. Mean monthly precipitation that falls as snow and simulated ranges (2030, 2060, and 2090) using the five GCMs and three emission scenarios for the three baseline conditions: (a) 1994, (b) 1989, and (c) 1970.

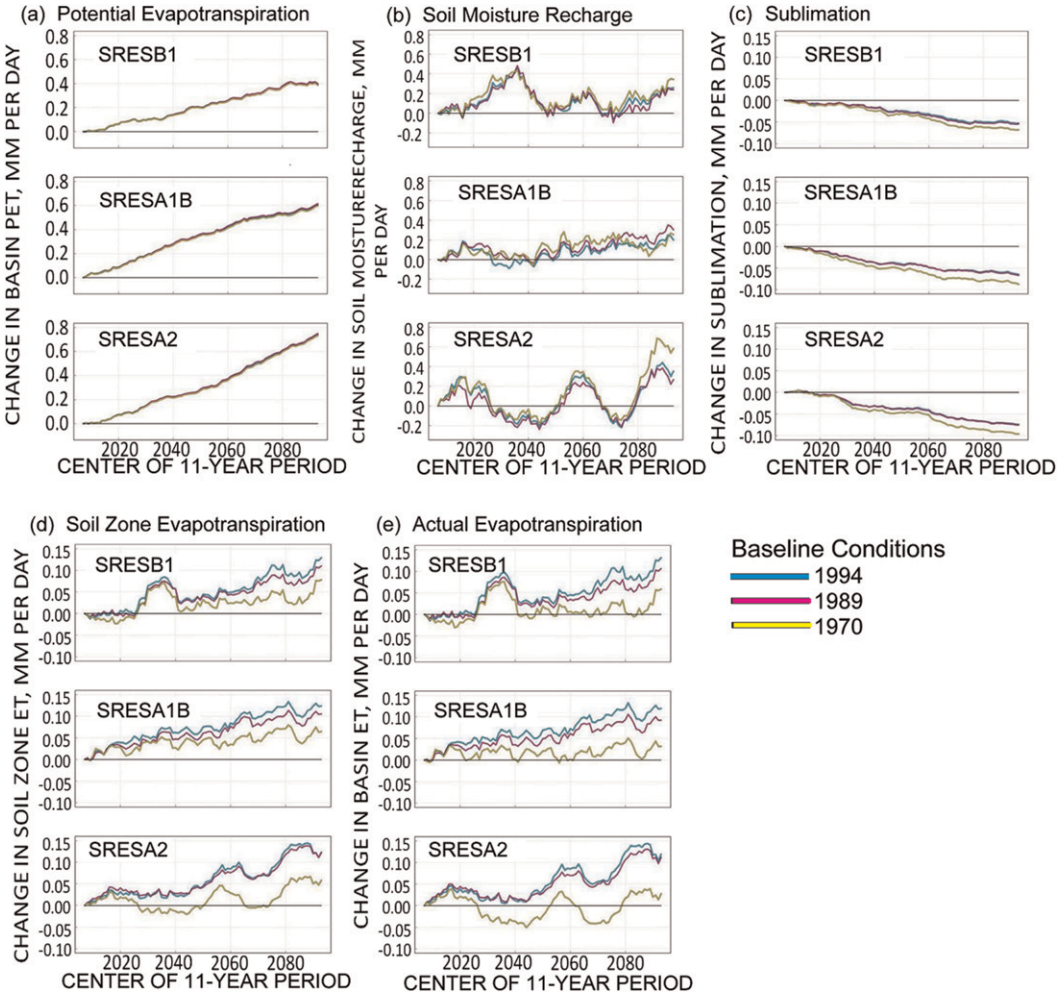

Figure 11. Simulated change in central tendency in 11-yr moving averages of (a) PET, (b) soil-moisture recharge, (c) sublimation, (d) soil zone evapotranspiration, and (e) AET by emission scenario using the 1994, 1989, and 1970 baseline conditions.

condition (1970) indicate substantially smaller increases than those using the warm PDO baselines (1994 and 1989; Figure 11d).

4.4. Streamflow simulations

The simulated change in the central tendency of the 11-yr moving averages of total streamflow and the components of flow (surface, subsurface, and groundwater) are shown in Figure 12 (see Markstrom et al. 2008 for the definition of these components). Simulations of streamflow are variable, showing both increases and decreases in the central tendencies of simulated streamflow. Simulated trends are similar, regardless of the baseline conditions used (Figure 12a). However, simulations from the cool PDO baseline condition (1970) show more severe changes

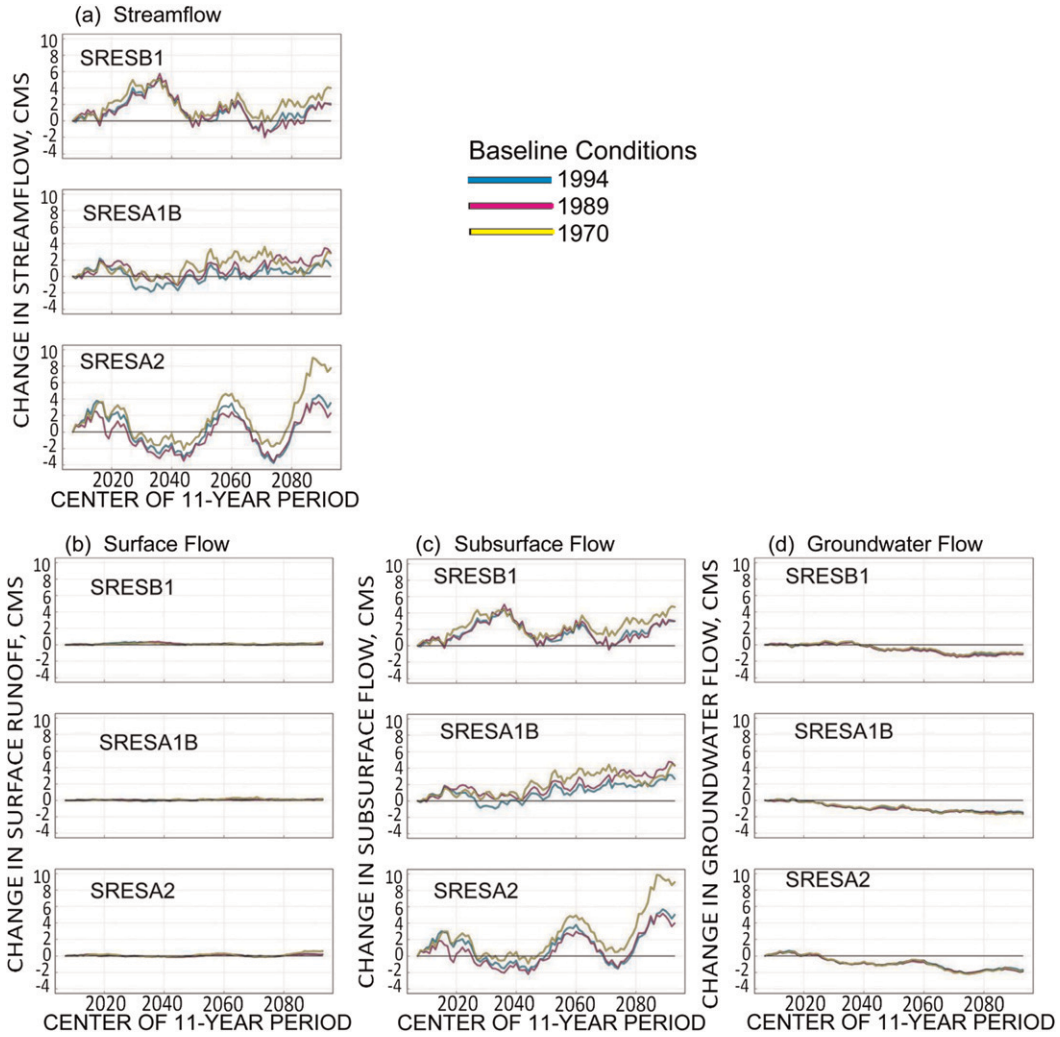

Figure 12. Simulated change in central tendency in 11-yr moving averages of (a) streamflow and the corresponding components of flow, (b) surface, (c) subsurface, and (d) groundwater, by emission scenario using the 1994, 1989, and 1970 baseline conditions.

than simulated from the warm PDO baselines (1989 and 1994). Minimal change is simulated in surface runoff (Figure 12b). Subsurface flow shows the greatest variability between emission scenarios and baseline conditions, indicating a relatively steady overall increase by the end of the twenty-first century for the A1B emission scenario only. All emission scenarios and baseline conditions indicate a similar steady decrease in groundwater flow by the end of the twenty-first century (Figure 12d).

Simulated annual streamflow shown in Figure 13 shows the range of uncertainty from the different sources (PRMS simulations, GCM projections, and baseline conditions) accounted for in this study (see Hay et al. 2011). The range of uncertainty shown in the ensemble of PRMS simulations from GCM projections of

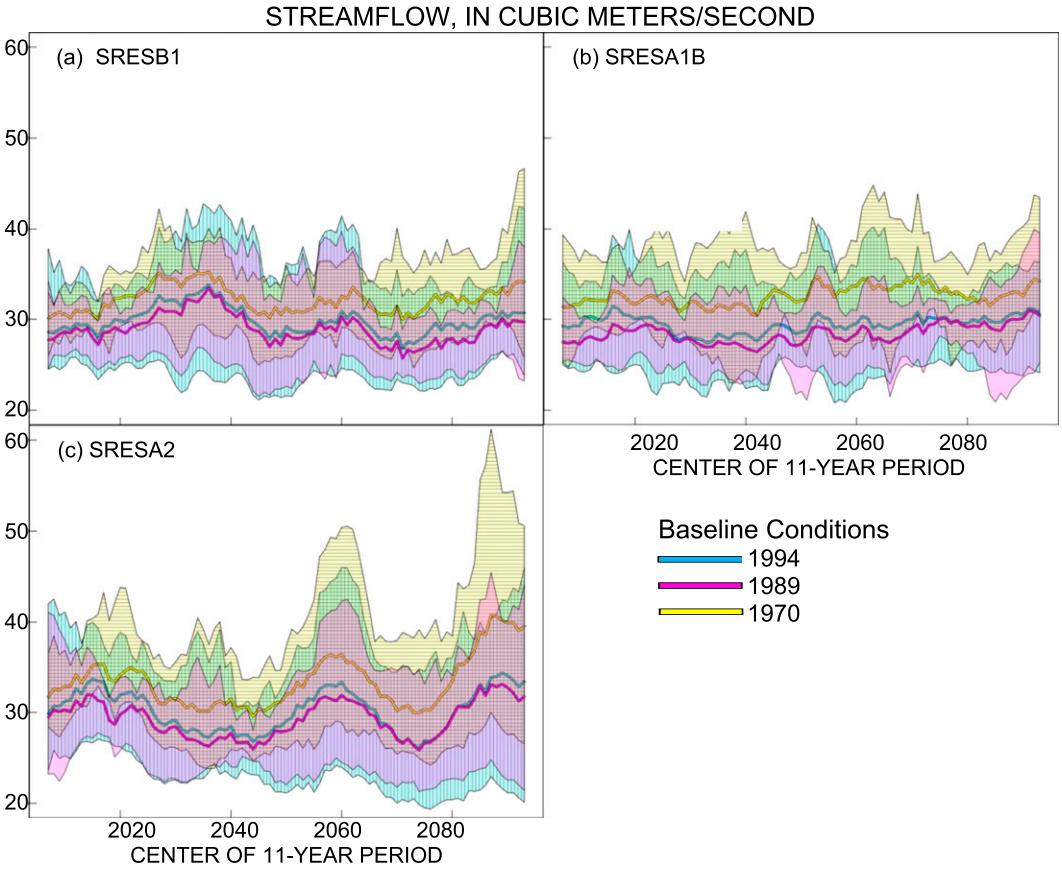

Figure 13. Simulated range in 11-yr moving averages of streamflow for emission scenarios (a) B1, (b) A1B, and (c) A2 using the 1994, 1989, and 1970 baseline conditions.

the carbon emission scenarios (see Murphy et al. 2004; Boorman and Sefton 1997; Alley et al. 2007) is consistently greater than the range of uncertainty from the hydrologic model or the variability within measured climate data (see Prudhomme and Davies 2009). An additional source of uncertainty, accounted for in this study and illustrated in Figure 13, is the selection of the baseline period. For example, the inclusion of the 1970 baseline period (cool PDO) results in greater uncertainty toward the end of the twenty-first century as compared with PRMS simulations from the other baselines (warm PDO). The combined range of uncertainty simulated from all baseline conditions represents a more realistic range of uncertainty for PRMS simulations of the GCM projections.

4.5. Regression analysis

Table 3 shows the results of a regression analysis based on the central tendencies of the five GCM model output sets for each of the three emission scenarios and baseline conditions. The twenty-first-century change (slope) is the change in the

central tendency of the specified variable per 11-yr moving average; values set in bold indicate a significant positive trend (at a probability level less than 0.05) and values set in italics indicate a significant negative trend (at a probability level less than 0.05), accounting for effects of lag-1 autocorrelation on the degrees of freedom (see Lettenmaier 1976; McCabe and Wolock 1997). The associated adjusted coefficient of determination (R^2) value gives an indication of the variability in the central trend [i.e., the higher the adjusted R^2 (adjR2) value, the less variability in the central tendency over time]. In all cases, when a significant trend was detected in the mean annual values of PRMS output variable, the direction of the trend remains constant for all baseline conditions, although the magnitudes vary.

A positive precipitation trend was found only for the A1B scenario using the 1970 (cool PDO) and 1989 (warm PDO) baseline conditions (Table 3a). The higher adjusted R^2 values for the A1B emission scenario indicate that the variability in the precipitation for the A1B scenario is substantially less than for the A2 and B1 scenarios (Figure 8).

Changes in the central tendencies of both maximum and minimum daily temperature are similar because the change-factor downscaling method applies the same change in mean monthly temperatures to each baseline (Tables 3b,c) (Hay et al. 2011). Also of note are similarities in the magnitude of changes projected for maximum and minimum temperature. In this study, the Jensen–Haise method is used to estimate PET (see Hay et al. 2011). Because the Jensen–Haise method uses temperature to estimate PET, projected increases in temperature will result in corresponding increases in PET (Table 3d and Figure 11a); however, changes in AET are not consistent between emission scenarios or baseline conditions (Table 3e and Figure 11e). Significant increases in AET are only simulated for the 1994 (A1B and A2) and 1989 (A1B) scenarios. One interpretation of this may be that the effect of baseline conditions on any particular PRMS output variable seems to be amplified in those hydrologic variables, which accumulate over time, or are constrained by storage limitations, such as limiting soil-moisture storage.

No significant trends were simulated for total streamflow (Table 3f). The low R^2 values suggest high variability in the central tendency simulations of streamflow over time. Components of flow show similar trend directions for the subsurface and groundwater flow using the three baseline conditions (Tables 3h,i). The magnitudes of the positive trends in subsurface flow differ between baselines (Table 3h and Figure 12c). The magnitudes of the negative trends in groundwater flow are similar (Table 3i and Figure 12d).

All GCM projections of future climate, when downscaled to the baseline conditions, produce significant negative trends in the proportion of precipitation that falls as snow, snow-covered area, snowpack water equivalent, and snowmelt (Tables 3j–m), but the magnitude of these negative trends can be substantially different between baseline conditions; larger decreases in snowpack water equivalent are simulated using the 1970 baseline conditions (cool PDO), and corresponding smaller decreases are simulated in snowmelt (less snowpack to melt).

5. Conclusions

The sensitivity in the simulated hydrologic response of the Almanor Catchment, North Fork of the Feather River, California, to three different baseline conditions

used in climate-change projections was evaluated using a PRMS watershed hydrology model. Comparison of the results from the three different baseline conditions resulted in the following conclusions: 1) the selection of the baseline period is an important source of uncertainty associated with the change-factor downscaling of projected future climates, 2) uncertainty due to the baseline period is not the same for all hydrologic variables, and 3) the location and physical characteristics of the study site may affect the sensitivity of some hydrologic variables to a particular baseline condition.

When using the change-factor method for downscaling, several baseline conditions may need to be chosen to represent a range in historical climatic conditions. It is important to evaluate and understand the trends, variability, and extremes in the historical climate record to determine this range. Just as multiple carbon emission scenarios simulated with an ensemble of GCMs can provide a sense of the uncertainty associated with a climate projection, an ensemble of baseline conditions also needs to be considered.

One of the more interesting aspects of this study was that not all hydrologic variables were equally sensitive to the selection of baseline conditions. PRMS variables that are not directly associated with long-term water storage in the model, such as PET, tend to be dominated by the climate trends introduced by the emission scenario. However, variables associated with interannual water storage in the model, like soil-moisture content, are sensitive to the selection of baseline conditions.

The geographic location in relation to local climate and the physical characteristics of the catchment may have an influence on the sensitivity of some hydrologic variables to a particular baseline condition. The Almanor Catchment is located in storm paths that result in large multidecadal variability in precipitation amounts. Topographically, it is bisected by the seasonal snow line. Slight changes in winter temperatures result in a change in precipitation form and, consequently, earlier or later peak runoff. In this paper, we show that trends in streamflow and related hydrologic components are simulated differently from cool (1970) and warm PDO baseline conditions (1989 and 1994). An important question to consider then is whether other watersheds in different geographic or topographic regimes show a similar sensitivity to the selection of baseline conditions.

Acknowledgments. The authors gratefully acknowledge the staff and funding contributions of California Department of Water Resources Division of Flood Management Hydrology Branch (DWR). The USGS, in cooperation with DWR, completed the Feather River Basin PRMS, which is the foundation model for this study. The DWR also provided funding towards the study described herein.

References

Alley, R. B., and Coauthors, 2007: Summary for policymakers. *Climate Change 2007: The Physical Science Basis,* S. Solomon et al., Eds., Cambridge University Press, 18 pp.

Arnell, N. W., 2003a: Effects of IPCC SRES emissions scenarios on river runoff: A global perspective. *Hydrol. Earth Syst. Sci.,* **7,** 619–641.

——, 2003b: Relative effects of multi-decadal climatic variability and changes in the mean and variability of climate due to global warming: Future streamflows in Britain. *J. Hydrol.,* **270,** 195–213.

——, and N. S. Reynard, 1996: The effects of climate change due to global warming on river flows in Great Britain. *J. Hydrol.,* **183,** 397–424.

Boorman, D. B., and C. E. M. Sefton, 1997: Recognizing the uncertainty in quantification of the effects of climate change on hydrological response. *Climatic Change,* **35,** 415–434.

Dettinger, M. D., D. R. Cayan, M. K. Meyer, and A. E. Jeton, 2004: Simulated hydrologic responses to climate variations and change in the Merced, Carson, and American River basins, Sierra Nevada, California, 1900-2099. *Climatic Change,* **62,** 283–317.

Diaz-Nieto, J., and R. L. Wilby, 2005: A comparison of statistical downscaling and climate change factor methods: Impacts on low flows in the River Thames, United Kingdom. *Climatic Change,* **69,** 245–268.

Durrell, C., 1987: *Geologic History of the Feather River Country, California*. University of California Press, 337 pp.

Eckhardt, K., and U. Ulbrich, 2003: Potential impacts of climate change on groundwater recharge and streamflow in a central European low mountain range. *J. Hydrol.,* **284,** 244–252.

Fowler, H. J., S. Blenkinsopa, and C. Tebaldi, 2007: Review. Linking climate change modelling to impacts studies: Recent advances in downscaling techniques for hydrological modelling. *Int. J. Climatol.,* **27,** 1547–1578.

Hay, L. E., and G. J. McCabe, 2010: Hydrologic effects of climate change in the Yukon River basin. *Climatic Change,* **100,** 509–523.

——, R. L. Wilby, and G. H. Leavesley, 2000: A comparison of delta change and downscaled SRES emission scenarios for three mountainous basins in the United States. *J. Amer. Water Resour.,* **36,** 387–397.

——, S. L. Markstrom, and C. Ward-Garrison, 2011: Watershed-scale response to climate change through the twenty-first century for selected basins across the United States. *Earth Interactions,* **15.** [Available online at http://EarthInteractions.org.]

Khan, M. S., P. Coulibaly, and Y. Dibike, 2006: Uncertainty analysis of statistical downscaling methods. *J. Hydrol.,* **319,** 357–382.

Koczot, K. M., A. E. Jeton, B. J. McGurk, and M. D. Dettinger, 2005: Precipitation-runoff processes in the Feather River Basin, northeastern California, with prospects for streamflow predictability, water years 1971-97. U.S. Geological Survey Scientific Investigations Rep 2004-5202, 82 pp.

Leavesley, G. H., R. W. Lichty, B. M. Troutman, and L. G. Saindon, 1983: Precipitation-Runoff Modeling System—User's manual. U.S. Geological Survey Water-Resources Investigation Rep. 83-4238, 207 pp.

Lettenmaier, D. P., 1976: Detection of trends in water quality data from records with dependent observations. *Water Resour. Res.,* **12,** 1037–1046.

Mantua, N. J., S. R. Hare, Y. Zhand, J. M. Wallace, and R. C. Francis, 1997: A Pacific interdecadal climate oscillation with impacts on salmon production. *Bull. Amer. Meteor. Soc.,* **78,** 1069–1079.

Markstrom, S. L., R. G. Niswonger, R. S. Regan, D. E. Prudic, and P. M. Barlow, 2008: GSFLOW—Coupled ground-water and surface-water flow model based on the integration of the Precipitation-Runoff Modeling System (PRMS) and the Modular Ground-Water Flow model (MODFLOW-2005). U.S. Geological Survey Techniques and Methods 6-D1, 240 pp.

McCabe, G. J., and D. M. Wolock, 1997: Climate change and the detection of trends in annual runoff. *Climate Res.,* **8,** 129–134.

Murphy, J. M., D. M. H. Sexton, D. N. Barnett, G. S. Jones, M. J. Webb, M. Collins, and D. A. Stainforth, 2004: Quantification of modelling uncertainties in a large ensemble of climate change simulations. *Nature,* **430,** 768–772.

Pilling, C., and J. A. A. Jones, 1999: High resolution equilibrium and transient climate change scenario implications for British runoff. *Hydrol. Processes,* **13,** 2877–2895.

Prudhomme, C., and H. Davies, 2009: Assessing uncertainties in climate change impact analyses on the river flow regimes in the UK. Part 1: Baseline climate. *Climatic Change,* **93,** 177–195.

——, N. Reynard, and S. Crooks, 2002: Downscaling of global climate models for flood frequency analysis: Where are we now? *Hydrol. Processes,* **16,** 1137–1150.